Interferometric switching of coherent anti-Stokes Raman scattering signals in microscopy

Alexei Nikolaenko, Vishnu Vardhan Krishnamachari, and Eric Olaf Potma[*]
Department of Chemistry, Natural Sciences II, University of California, Irvine, California 92697, USA
(Received 8 July 2008; revised manuscript received 23 November 2008; published 27 January 2009)

Coherent anti-Stokes Raman scattering (CARS) interferometry is used to deplete the anti-Stokes radiation emerging from a tightly focused spot. Near-to-complete depletion of the anti-Stokes radiation is obtained when a phase-controlled local oscillator field at the anti-Stokes frequency is out of phase with the induced CARS field in the focal volume. Unlike in traditional interferometry, this depleted energy is not spatially redistributed. A theoretical analysis shows that the energy loss in the anti-Stokes channel is accompanied by an energy gain in the pump and Stokes channels. Interferometric switching of anti-Stokes radiation may offer a route toward developing high-resolution CARS microscopy.

I. INTRODUCTION

In optical microscopy, imaging is achieved by collecting the optical response from the sample at spatially separated points. It is often helpful to control the nature of the material's optical response for the purpose of improving the imaging contrast or resolution. In fluorescence microscopy, the ability to control the fluorophore's response has been key to the development of resolution enhancement techniques. For instance, photoswitching of the fluorophore's emission, whereby the optical response from sample chromophores is switched on and off with optical radiation in a controlled fashion, forms the basic mechanism for resolution enhancement in photoactivated localization microscopy (PALM) [1] and sub-diffraction-limited imaging by stochastic optical reconstruction microscopy (STORM) [2]. Another example of fluorescence emission control is found in stimulated emission depletion (STED) microscopy [3,4]. STED achieves resolution enhancement by switching off the fluorescence from selected parts of the focal volume with a precisely controlled depletion beam.

The success of the resolution enhancement techniques in fluorescence relies on the ability to control the emissive properties of fluorophores with optical radiation independent of the excitation illumination. Fluorescence control is facilitated by the existence of several mechanisms to manipulate the radiative relaxation from the excited state of the fluorophore. Both the direct alteration of the excited state through photochemical switching, as used in PALM and STORM, and the selected depopulation of the excited state, employed in STED, provide a controlled handle for switching the fluorescence response.

Similar control of light emission would also be beneficial to improve the imaging capabilities in coherent anti-Stokes Raman scattering (CARS) microscopy, an emerging nonlinear imaging tool with biological and biomedical applications [5,6]. CARS employs a pump and a Stokes beam of frequency ω_1 and ω_2, respectively, to drive a vibrational coherence at $\omega_1-\omega_2$. The molecular vibrations are probed through a subsequent interaction with the pump, generating a coher-

ent signal at the anti-Stokes frequency $\omega_3=2\omega_1-\omega_2$. However, currently no technique has been reported that enables optically controlled switching of the coherent emission in CARS microscopy.

Unlike fluorescence, the CARS process does not rely on the population of an electronic state of the target molecule. CARS is a parametric process in which no energy is transferred from the light fields to the molecule. While CARS is sensitive to vibrational molecular eigenstates, it follows from a density matrix description that the CARS process is the result of light-mediated coherent coupling of molecular states rather than the creation of a vibrational population. Without the involvement of an excited-state population, either vibrational or electronic, the manipulation tools developed for fluorescence microscopy are not applicable to CARS microscopy. Note that similar arguments hold for imaging based on second-harmonic generation (SHG), which, like CARS, is also a coherent process independent of an excited state population.

The development of a switching mechanism in CARS microscopy would be an important first step towards possible resolution enhancement techniques in coherent nonlinear imaging. Because CARS is different from fluorescence, different forms of signal manipulation have to be explored. One possible route is to achieve switching through depletion of the vibrational coherence by means of a subsequent coherent Raman process. Unlike an electronic population, however, the vibrational coherence has a precisely defined phase, which inherently introduces interference effects during a depleting coherent Raman interaction. The inherent interference complicates the effective depletion of the vibrational coherence. Another complication is that a second coherent Raman interaction is rather undesirable in terms of sample illumination. Indeed, such an interaction would involve an additional pair of laser pulses of moderately high energy, comparable to that of the pump and the Stokes pulse pair, which increases the likelihood of photodamage in biological samples.

In this paper we explore a mechanism for controlling CARS which is not based on manipulating the process at the level of the vibrational coherence, but rather at the level of the radiation process. The idea is simple: a low-power (pW–nW range) local oscillator field at the anti-Stokes frequency ω_3 is allowed to mix with the pump and Stokes fields

---
*epotma@uci.edu

in a sample in collinear fashion. Importantly, the chosen power range of the local oscillator beam is generally more than six orders of magnitude lower than the incident pump and Stokes beams, and is thus not inflicting any damage to the sample. When the local oscillator is in phase with the ensuing anti-Stokes radiation generated by the pump and the Stokes fields, an enhanced signal at frequency ω_3 is expected. On the other hand, when the local oscillator is out of phase with the induced anti-Stokes polarization, a depleted signal is expected. Related ideas have been exploited in designing nonlinear mirrors that reflect selected Raman-shifted components based on nonlinear interference effects [7] and in suppressing the nonresonant background in CARS spectroscopy [8,9]. Recently, the idea of interference with a local oscillator was also introduced in the field of CARS microscopy as a tool for detecting the real and imaginary parts of the signal, with applications both in imaging [10–12] and in microspectroscopy [13–17].

In this work we show that it is possible to completely switch off the anti-Stokes radiation from the focal volume with a local-oscillator beam of minute pulse energy. We experimentally demonstrate the depletion of anti-Stokes radiation in an optical microscope in a robust and fully-phase-controlled manner. To explain these observations, we furthermore performed a theoretical analysis based on a coupled-wave-equation approach. Our calculations confirm that in this form of CARS interferometry, a local-oscillator beam can fully control the energy flow between the pump, Stokes, and anti-Stokes radiation channels. By controlling the phase and amplitude of the local oscillator, we show that the anti-Stokes emission channel can be completely depleted and that the energy is subsequently diverted to the pump and Stokes radiation channels. This study sets the stage for more advanced degrees of CARS emission control, in which radiation emerging from selective parts of the focal volume is nulled for the purpose of resolution enhancement.

II. EXPERIMENTAL LAYOUT

A schematic of the experimental setup is given in Fig. 1. The setup consists of a picosecond Nd:vanadate-pumped optical parametric oscillator system that delivers a high-repetition-rate pump beam at 812 nm and a Stokes beam at 1064 nm. Details of the light source can be found elsewhere [18]. The pump and Stokes beams are collinearly combined and overlapped in time before entering the interferometer. In one arm of the interferometer a local oscillator is generated by focusing the pump and Stokes beams into a solution of dimethyl sulfoxide (DMSO). Since the frequency difference between the pump and Stokes equals the 2913-cm^{-1} CH$_3$ vibration in DMSO, a strong local oscillator is generated at the anti-Stokes frequency. The other arm of the interferometer provides the delay for the pump and Stokes beams. The local oscillator is collinearly combined with the pump and Stokes on a dichroic mirror and directed towards the microscope (Fluoview 300, Olympus).

The interferometer is stabilized by a 532-nm continuous-wave reference laser. The reference laser beam is coupled to the interferometer through the main beam splitter and travels
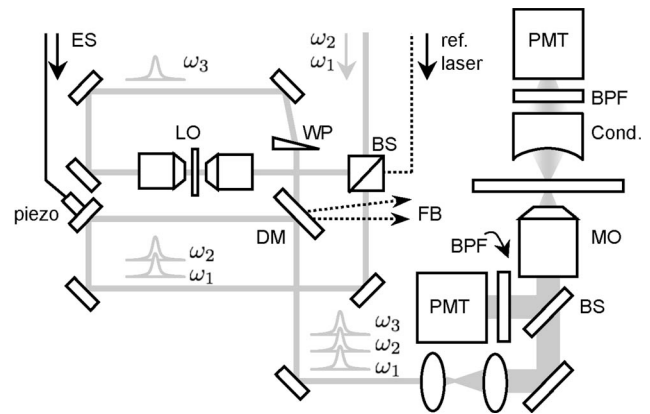

FIG. 1. Schematic of the setup. The setup is comprised of an interferometer and a microscope. The interferometer is stabilized by the reference laser. ES, error signal; LO, unit for generating local oscillator; WP, wedged plate; BS, 50-50 beam splitter; DM, dichroic mirror; FB, optical feedback signal; MO, microscope objective; BPF, bandpass filter; Cond., condenser; PMT, photomultiplier.

the same path as the other beams through each of the arms. In the local oscillator arm, a wedged plate is placed to introduce an angular difference between the local oscillator and the reference beam at the dichroic mirror, resulting in a fringe pattern on the 532-nm beam. Changes in the fringe pattern serve as the source for a computer-synthesized error signal which is used to correct the interferometer's path length difference with a mirror-mounted piezoactuator. Importantly, the interferometer can be phase stabilized at any arbitrary, computer-controlled phase setting of the local oscillator. Phase stabilization down to path length fluctuations of ~5 nm is achieved with this scheme, which is sufficient for CARS interferometry. More details on the interferometer can be found in Ref. [19].

The pump, Stokes, and local oscillator beams are focused with a 1.15-NA water immersion lens to a sub-μm focal spot in a sample of DMSO. The incident beam powers at the sample for the pump and Stokes are about 10 mW, while the local-oscillator average beam power amounts to only a few hundreds of picowatts. The total anti-Stokes radiation is captured with a 0.55-NA condenser in the forward direction, filtered through two bandpass filters (650 ± 20 nm, Chroma) and detected by a photomultiplier (R3896, Hamamatsu). Anti-Stokes radiation in the epi-direction was detected by introducing a 50/50 beam splitter in the microscope beam path. Backward propagating light is reflected off the beam splitter, spectrally filtered using a similar set of bandpass filters, and detected with a second photomultiplier.

III. EXPERIMENTAL RESULTS

The ability to deplete anti-Stokes radiation is shown in Fig. 2. The pump and Stokes beams generate CARS from the CH$_3$ stretching vibration of DMSO at 2913 cm^{-1}. When the phase-stabilized local oscillator is added with an intensity comparable to the CARS signal emerging from the focal volume, a clear interference between the CARS signal and the local oscillator is observed. To visualize the interference, the
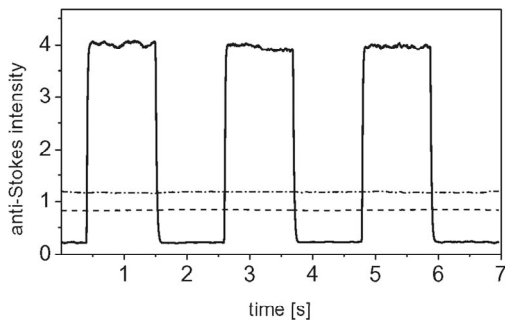
FIG. 2. Dependence of the coherent anti-Stokes signal as a function of the local-oscillator phase. Solid line is the total anti-Stokes signal. The dashed line is the CARS signal from DMSO at 2913 cm^{-1}, and the dash-dotted line is the local-oscillator intensity. Phase of the local oscillator was periodically toggled between 0 and π by the computer-controlled interferometer. The high plateau of the total anti-Stokes signal corresponds to $\phi=0$, and the low plateau corresponds to $\phi=\pi$. Note that fluctuations are due to laser instabilities rather than phase fluctuations.

phase of the local oscillator is computer controlled and toggled between two different values at periodic intervals. At the DMSO resonance, a maximum intensity is seen when the phase difference ϕ between the local oscillator and the CARS radiation is zero. When the phase-difference is set to $\phi=\pi$, the signal at the anti-Stokes frequency is minimized.

It is tempting to analyze the interference of the anti-Stokes components in a similar fashion as in a standard interferometer. In this case, one would consider two phase coherent fields, a CARS field E_{as} and a local oscillator E_{lo}, which are combined on a beam splitter and allowed to interfere. The resulting intensity measured in one of the transmission directions after the beam splitter is then $I=|E_{as}+E_{lo}e^{-i\phi}|^2$. Applying such an analysis to the data in Fig. 2 yields that the interference contrast $4E_{as}E_{lo}$ is 95% of the predicted value, indicating that the interference between the two components is almost complete. Achieving such a high level of interference contrast in the focus of a high-numerical-aperture lens is encouraging given the sensitivity of the process to the quality of the wave fronts. Further control of the beam quality is expected to lead to depletion efficiencies of 100%. If needed, the wave front of the local oscillator can be shaped with a spatial light modulator to optimize complete interference throughout the focal volume.

Although intuitive, this simple interferometer model is unable to explain the nature of the interaction between the field components in focus. This shortcoming is most obvious when considering the phase setting $\phi=\pi$ and the anti-Stokes radiation is largely depleted. The simple interferometer model predicts that the depleted energy in one of the propagation directions (transmission) after the beam splitter is retrieved in the other propagation direction (reflection), while the total energy is conserved. In the CARS interferometry experiment, however, the depleted anti-Stokes radiation in the forward-propagation direction is not retrieved in the epi-direction. For instance, we have simultaneously measured the anti-Stokes light in the epi-mode and observed that the loss of radiation at the anti-Stokes frequency in the forward direction is not compensated by a gain in the backward di-

rection. In fact, the epi-CARS signal showed the same type of local oscillator phase dependence as observed in the forward direction. Another potential explanation for the observed signal depletion is a possible change in the phase-matching condition for the CARS radiation. Altered phase-matching conditions typically produce CARS emission patterns that are notably different from the on-axis propagation of the phase-matched CARS radiation. However, we found no evidence for altered phase-matching conditions in the forward direction upon switching the phase of the local oscillator, as no enhanced forward CARS radiation was detected at angles different from the on-axis phase-matched direction.

A more complete picture of the interacting field components is required to describe the flow of energy in the anti-Stokes channel. This picture considers the phase coherent local oscillator as part of the pump- and Stokes-induced light-matter interactions in the focal volume. Unlike a beam splitter in linear interferometry, which distributes energy into different propagation directions without affecting the color of the light, the medium in CARS interferometry can mediate the energy exchange between the participating frequencies. The flow of energy from the anti-Stokes channel to the other frequency channel leads to subtle changes of the pump and Stokes beam intensities. Nonetheless, the measurement of these subtle changes would require a high detection sensitivity with a vast dynamic range (from picowatts to tens of milliwatts), which is far beyond our detection capabilities. In order to better understand the energy exchange among the different channels and explain our experimental observations, we have performed a detailed theoretical analysis of the light-matter interactions.

IV. THEORETICAL ANALYSIS

In modeling the interactions between the pump, Stokes, and Raman-shifted frequency components, we adopt a plane-wave approximation. Such an assumption is reasonable even in the case of tightly focused fields, as the lateral dimension that is ignored in the case of plane waves is not expected to alter the processes of energy transfer between the participating waves in a fundamental way. Our treatment largely follows the framework of Druet and Taran [20]. Related descriptions of the interacting waves in the CARS process can be found in Refs. [7,21]. An important distinction between previous studies on CARS coupled wave equations and our discussion here is that we explicitly consider the influence of a phase-adjustable local oscillator on the CARS process. In the Appendix, we derive comprehensive coupled-wave equations for describing the full set of third-order Raman interactions between the pump (ω_1), Stokes (ω_2), anti-Stokes ($\omega_3=2\omega_1-\omega_2$), and coherent Stokes ($\omega_4=2\omega_2-\omega_1$) fields in the presence of an anti-Stokes local oscillator.

Figure 3 shows simulation results of the relative intensity of the anti-Stokes radiation upon propagating a distance corresponding to the focal depth of a high-numerical-aperture lens (≈ 1 μm). Here $\omega_1-\omega_2$ is set to the molecular resonance ω_0. At $z=0$, the onset of the nonlinear interaction volume, the anti-Stokes radiation equals the intensity of the local oscilla-
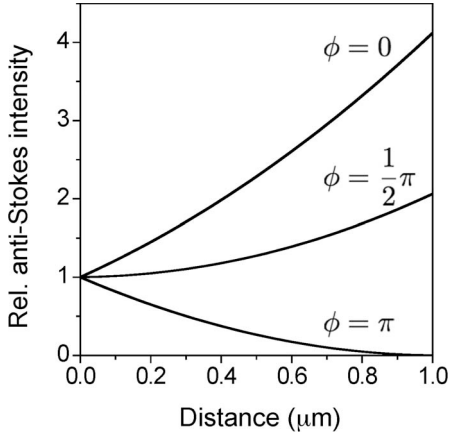
FIG. 3. Simulation of the total anti-Stokes signal as a function of propagation distance for various settings of the local-oscillator phase. It is assumed that $\omega_1 - \omega_2 = 2913$ cm^{-1}. In the calculations $E_{lo}(0)$ was set equal to the CARS signal $E_{as}(z_{max})$.

tor. Upon propagation, the anti-Stokes amplitude is affected by the pump- and Stokes-induced polarization at ω_3. When $\phi_3(0) = \pi/2$, no interference occurs between the seed light and the induced radiation, and the total anti-Stokes radiation is an addition of the local oscillator and the CARS intensity. In this simulation, we have set the total generated CARS intensity to be equal to the initial local-oscillator intensity— i.e., $E_{as} = E_{lo}$. The situation is different when $\phi_3(0) = 0$, when the total anti-Stokes radiation grows much faster then what one would expect from a simple addition. This nonlinear growth is analogous to the constructive interference of two field components in the simple interferometer model, yielding a total anti-Stokes intensity of $I \approx I_{as} + I_{lo} + 2|E_{as}E_{lo}|$ at the end of the interaction volume. For $\phi_3(0) = \pi$, the seed light is out of phase with the pump- and Stokes-induced polarization and the total anti-Stokes radiation is depleted. Note that the depletion is complete in the condition $E_{as} = E_{lo}$. In the case $E_{as} \neq E_{lo}$, the depletion is incomplete, but is still substantial over a tolerable range in the vicinity of $E_{as} \approx E_{lo}$. This loss of anti-Stokes energy is compensated by a gain in the other frequency channels.

In Fig. 4, we investigate how the energy is redistributed over the different channels as a function of the local-oscillator phase. While the anti-Stokes radiation peaks when $\phi = 0$ and is maximally depleted when $\phi = \pi$, the radiation in the CSRS channel is hardly affected. This is an expected result, as the effect of changes in the anti-Stokes channel on the ω_4 wave is mediated by the $A_1 A_2 A_3^*$ term [see Eq. (A10)], which is orders of magnitude weaker than main driving term $A_1^* A_2 A_2$. From Fig. 4(b), it is evident that the pump and Stokes channels display a significant relative change upon varying the local-oscillator phase. Both the ω_1 and ω_2 waves decrease in amplitude when the anti-Stokes radiation is maximized and show a relative gain when the anti-Stokes channel is depleted. However, the Stokes channel is much more affected than the pump channel. This can be explained by considering the dominant mixing terms between the anti-Stokes field and the pump and Stokes fields, respectively.

The dominant contribution of the E_3 field to the Stokes field is mediated through $\chi^{(3)}(\omega_2 = -\omega_3 + \omega_1 + \omega_1)$. Even
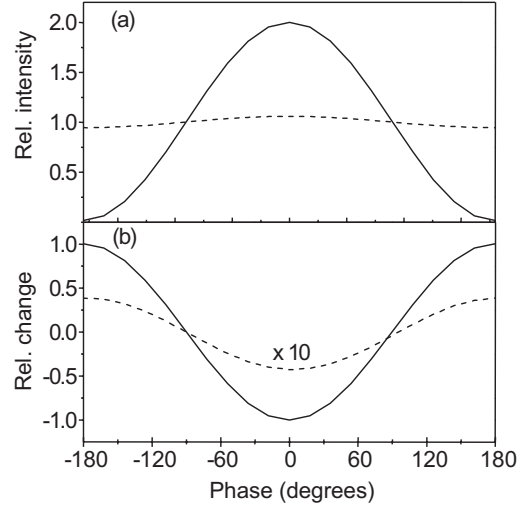

FIG. 4. (a) Dependence of the anti-Stokes signal (solid line) on the local oscillator phase under resonant conditions. The coherent Stokes component is indicated by the dashed line. (b) Relative depletion of the pump (dashed line) and Stokes (solid line) intensities as a function of the local-oscillator phase under resonant conditions. In the calculations $E_{lo}(0)$ was set equal to the CARS signal $E_{as}(z_{max})$.

though the E_3 field is weak, this process gains importance because the resulting radiation at ω_2 is homodyned by the strong Stokes incident field. On the other hand, the anti-Stokes field participates in the generation of the pump light through two dominant $\chi^{(3)}$ processes: $\chi^{(3)}(\omega_1 = \omega_3 - \omega_1 + \omega_2)$ and $\chi^{(3)}(\omega_1 = -\omega_1 + \omega_2 + \omega_3)$. The joint contribution of these terms has a weight of $2s + S + S^*$. Nonetheless, at a vibrational resonance, $S^* = -S$ and the resonant parts of these $\chi^{(3)}$ terms destructively interfere. The pump beam is thus much less affected by E_3 mixing than the Stokes beam. When tuning off the vibrational resonance by 100 cm^{-1} to lower energy, the phase dependence changes accordingly, as depicted in Fig. 5. Maximum anti-Stokes radiation is now observed for a phase setting that is shifted 90° relative to the resonant case. The pump and Stokes depletions follow a similar pattern. Because the destructive interference between the two dominant $\chi^{(3)}$ terms is now lifted, the E_3-mixing-induced changes in the pump and Stokes intensities are of comparable magnitude.

V. DISCUSSION

Our experiments demonstrate that a local oscillator can be used to switch off the anti-Stokes radiation emanating from the focal volume. Upon depletion of the forward-propagating anti-Stokes light, we have observed no enhanced radiation at the anti-Stokes frequency in any other direction. This suggests that CARS interferometry with a collinear local oscillator cannot be interpreted as a linear interferometry experiment. Instead, the local oscillator partakes in the third-order light-matter interactions and plays a role in controlling the energy flow between the participating waves. Our measurements thus point out an intrinsic difference between linear and nonlinear interferometries.
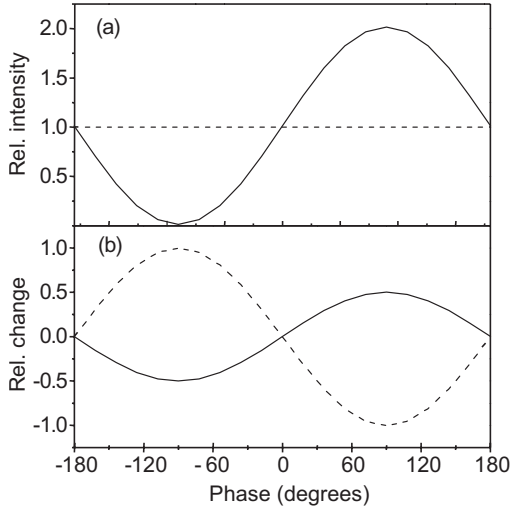
FIG. 5. (a) Dependence of the anti-Stokes signal (solid line) on the local oscillator phase under off-resonant conditions. The coherent Stokes component is indicated by the dashed line. (b) Relative depletion of the pump (dashed line) and Stokes (solid line) intensities as a function of the local-oscillator phase under off-resonant conditions. In the calculations $E_{lo}(0)$ was set equal to the CARS signal $E_{as}(z_{max})$.

The theoretical analysis based on coupled-wave equations reveals that at a vibrational resonance and a phase setting $\phi = \pi$, the loss in energy in the anti-Stokes channel is predominantly compensated by a gain in the Stokes radiation channel. The fact that much less energy is redirected to the pump channel is due to a interference between $\chi^{(3)}$ terms that produce anti-Stokes-mediated radiation at the pump frequency. This observation underlines the notion that the communication between the radiation channels should be understood as four-wave-mixing processes, even though the anti-Stokes field is more than six orders of magnitude weaker compared to the pump and Stokes channels. The fact that minute anti-Stokes field amplitudes can control the energy flow through nonlinear interactions in the CARS process is explained by the strong homodyne amplification of certain $\chi^{(3)}$ terms.

The significance of this work is that nonlinear interference is a feasible option for fully controlling the anti-Stokes radiation in a tightly focused spot of an optical microscope. The near-complete interference with the local oscillator in the CARS process that we observed indicates that wave fronts can be managed well even in submicrometer-sized focal volumes. The level of emission control offered by CARS interferometry may be important for the development of superresolution in CARS microscopy. A possible route towards resolution enhancement is to employ phase-shaped local-oscillator beams that deplete selected parts of the CARS focal volume, an approach that bears resemblance to STED microscopy. However, there are important differences between the depletion mechanisms in CARS interferometry and STED. In CARS interferometry, the depletion mechanism discussed here cannot be driven into saturation. Resolution enhancement in STED is possible by virtue of saturating the depletion process [4]. On the other hand, in CARS

interferometry, not only can the amplitude profile of the depletion beam be controlled, but also its spatial phase. It is noteworthy to emphasize that focal beams can be dressed with sharp π-phase shifts which compartmentalize the focal volume into smaller segments, in which the molecules are driven at distinct phases. For instance, the sharp phase features of shaped focal fields form the operating principle for the contrast enhancement in focus-engineered CARS microscopy [22,23]. When combined with phase-shaped local oscillator beams, CARS interferometry provides a mechanism for detecting anti-Stokes radiation from a subset of focal phase segments, while the radiation from other compartments is depleted. This principle, which is absent in fluorescence microscopy, holds promise for improving the resolution in CARS imaging.

VI. CONCLUSION

In this work we demonstrate that anti-Stokes radiation emerging from a tightly focused spot can be completely switched off through an interferometric process. Using a stabilized, phase-adjustable interferometer, we achieved nearly complete interference between the local oscillator and the pump- and Stokes-induced CARS radiation. We verified that the depletion in the forward-propagating anti-Stokes channel is not compensated by an increased anti-Stokes emission in another direction. Instead, our theoretical analysis shows that depletion of the anti-Stokes radiation is accompanied by a gain in the pump and Stokes radiation channels. This implies that CARS interferometry provides a genuine switching mechanism for controlling the amount of anti-Stokes radiation from the focal volume by merely varying the phase of a weak (more than six orders of magnitude weaker than the pump and the Stokes fields) local-oscillator field. This work has set the stage for the next challenge: select depletion of parts of the focal volume using spatial-amplitude and spatial-phase shaping, such as used in focus-engineered CARS. Such schemes may play an important role in developing techniques for increased spatial resolution in CARS microscopy.

APPENDIX

We consider the pump (ω_1) and Stokes (ω_2) fields along with the frequency shifted $\omega_3 = 2\omega_1 - \omega_2$, which we refer to as CARS, and $\omega_4 = 2\omega_2 - \omega_1$, indicated here as the coherent Stokes Raman scattering (CSRS) component. The fields with frequencies ω_1, ω_2, ω_3, and ω_4 have wave vectors $\mathbf{k}_1$, $\mathbf{k}_2$, $\mathbf{k}_3$, and $\mathbf{k}_4$ with magnitudes of $k_1 = \omega_1 n_1 / c$, $k_2 = \omega_2 n_2 / c$, $k_3 = \omega_3 n_3 / c$, and $k_4 = \omega_4 n_4 / c$, where n_i ($i = 1, \ldots, 4$) are the refractive indices of the medium for the four fields, respectively, and c is the speed of light in vacuum. Assuming that

the fields propagate along positive z direction with polarization along the x direction, the electric field corresponding to the four frequencies can be written as

$$\mathbf{E}_j(z,t) = \frac{1}{2}[A_j(z)e^{i(k_jz-\omega_jt)} + A_j^*(z)e^{-i(k_jz-\omega_jt)}]\hat{\mathbf{i}}, \quad j=1,\dots,4.$$
(A1)

The amplitude and the phase of each of the waves will be affected upon traveling through the medium. The waves are coupled through the third-order polarization $\mathbf{P}^{(3)}$ of the medium, which enables the energy transfer among the waves. Assuming an isotropic and nonmagnetic medium, the propagation of each of the components is described by the wave equation

$$\nabla^2\mathbf{E} - \frac{n^2}{c^2}\frac{\partial^2}{\partial t^2}\mathbf{E} = \frac{1}{\epsilon_0 c^2}\frac{\partial^2}{\partial t^2}\mathbf{P}^{(3)}.$$
(A2)

The effect of the applied fields on the induced third-order polarization density is written as

$$\mathbf{P}^{(3)} = \epsilon_0\chi^{(3)}\mathbf{E}\cdot\mathbf{E}\cdot\mathbf{E},$$
(A3)

where ϵ_0 is the electric permittivity in vacuum and $\chi^{(3)}$ is the third-order susceptibility. We write the third-order susceptibility $\chi^{(3)}(\omega_3=\omega_1-\omega_2+\omega_1)=s+S$ as a sum of nonresonant (denoted by s) and resonant (denoted by S) parts. The nonresonant part is a real constant, whereas the resonant part is complex and has the form

$$S = \frac{G}{\omega_1-\omega_2-\omega_0+i\Gamma_0}.$$
(A4)

Here G is real and determines the strength of the third-order susceptibility near the resonance (when $\omega_1-\omega_2=\omega_0$). Following Druet and Taran [20], we note that the third-order susceptibility $\chi^{(3)}(\omega_4=\omega_2-\omega_1+\omega_2)$ is the complex conjugate of $\chi^{(3)}(\omega_3=\omega_1-\omega_2+\omega_1)$ since ω_1 and ω_2 combine as $\omega_2-\omega_1$. Based on this argument, we can write expressions for the third-order susceptibilities at other frequencies [for example, $\chi^{(3)}(\omega_4=\omega_1-\omega_3+\omega_2)=s+S^*$, $\chi^{(3)}(\omega_3=\omega_3-\omega_1+\omega_1)=s+S$, and so on].

We invoke the slowly varying wave approximation (SVWA) for wave propagation along one dimension. It has been shown that the SVWA provides a good description of the wave interactions even under the condition of tight focusing [24]. The left-hand side of Eq. (A2) for the ω_1 field can now be written as

$$\nabla^2 E_1(z,t) - \frac{n_1^2}{c^2}\frac{\partial^2}{\partial t^2}E_1(z,t) \approx ik_1\frac{\partial A_1(z)}{\partial z}e^{i(k_1z-\omega_1t)} + \text{c.c.}$$
(A5)

A full analysis of the energy transfer between the participating fields includes all interactions in the four-wave mixing of the fields ω_1, ω_2, ω_3, and ω_4. For instance, in calculating the component of the third-order polarization that oscillates at ω_1, not only the influence of the Stokes beam (through the stimulated Raman scattering process $\omega_1=\omega_1-\omega_2+\omega_2$) should be considered, but also the effect of the weak ω_3 and

ω_4 fields. In fact, frequency-mixing processes like $\omega_1=-\omega_1+\omega_2+\omega_3$ are crucial in understanding the local-oscillator-mediated energy transfer from the anti-Stokes channel to the pump channel. Including all such interactions, we find the third-order polarization density at ω_1:

$$\frac{8}{\epsilon_0}P^{(3)}(z,\omega_1) = (2s+S+S^*)A_1^*A_2A_3e^{i[-(k_1-k_2-k_3)z-\omega_1t]}$$
$$+ (s+S)A_2A_2A_4^*e^{i[(2k_2-k_4)z-\omega_1t]}$$
$$+ (s+S^*)A_2^*A_3A_4e^{-i[(k_2-k_3-k_4)z-\omega_1t]}$$
$$+ sA_1A_1A_1^*e^{i[k_1z-\omega_1t]} + (s+S)A_1A_2A_2^*e^{i(k_1z-\omega_1t)}$$
$$+ (s+S^*)A_1A_3A_3^*e^{i(k_1z-\omega_1t)} + sA_1A_4A_4^*e^{i(k_1z-\omega_1t)}$$
$$+ \text{c.c.}$$
(A6)

Using Eqs. (A2) and (A5), and adopting the expressions for the polarization density, we can write the differential equation for the change in the amplitude of the pump field as

$$-8i\frac{n_1c}{\omega_1}\frac{\partial A_1(z)}{\partial z} = (2s+S+S^*)A_1^*A_2A_3e^{-i\delta k_az}$$
$$+ (s+S)A_2A_2A_4^*e^{i\delta k_sz}$$
$$+ (s+S^*)A_2^*A_3A_4e^{-i(\delta k_a+\delta k_s)z} + sA_1A_1A_1^*$$
$$+ (s+S)A_1A_2A_2^* + (s+S^*)A_1A_3A_3^*$$
$$+ sA_1A_4A_4^*,$$
(A7)

where $\delta k_a=2k_1-k_2-k_3$ is the wave-vector mismatch between the CARS and the exciting fields and $\delta k_s=2k_2-k_1-k_4$ is the wave-vector mismatch between the CSRS and the exciting fields. Similarly, we have

$$-8i\frac{n_2c}{\omega_2}\frac{\partial A_2(z)}{\partial z} = (s+S^*)A_1A_1A_3^*e^{i\delta k_az}$$
$$+ (2s+S+S^*)A_1A_2^*A_4e^{-i\delta k_sz}$$
$$+ (s+S)A_1^*A_3A_4e^{-i(\delta k_a+\delta k_s)z}$$
$$+ (s+S^*)A_1A_1^*A_2 + sA_2A_2A_2^* + sA_2A_3A_3^*$$
$$+ (s+S)A_2A_4A_4^*,$$
(A8)

$$-8i\frac{n_3c}{\omega_3}\frac{\partial A_3(z)}{\partial z} = (s+S)A_1A_2A_4^*e^{i(\delta k_a+\delta k_s)z}$$
$$+ (s+S)A_1A_2^*e^{i\delta k_az} + (s+S)A_1A_1^*A_3$$
$$+ sA_2A_2^*A_3 + sA_3A_3^*A_3 + sA_3A_4A_4^*, \quad (A9)$$

$$-8i\frac{n_4c}{\omega_4}\frac{\partial A_4(z)}{\partial z} = (s+S^*)A_1^*A_2A_2e^{i\delta k_sz}$$
$$+ (s+S^*)A_1A_2A_3^*e^{i(\delta k_a+\delta k_s)z} + sA_1A_1^*A_4$$
$$+ (s+S^*)A_2A_2^*A_4 + sA_3A_3^*A_4 + sA_4A_4A_4^*.$$
(A10)

Equations $(A7)$–$(A10)$ form a complete set of coupled differential equations that describe all relevant interactions between the pump, Stokes, CARS, and CSRS fields. Numerical evaluation of the coupled differential equations is carried out in MATLAB. A single vibrational resonance at $\omega_0 = 2913$ cm^{-1} is considered, with $\Gamma = 10$ cm^{-1}. The pump was set to 812 nm and the Stokes to 1064 nm. To model the effect of the local oscillator, it is introduced as a seed wave at frequency ω_3 in Eq. $(A9)$. The amplitude $[|A_3(z=0)|]$ and phase $[\phi_3(z=0)]$ of the seed wave can be easily adjusted in simulating the nonlinear interactions.

[1] E. Betzig, G. H. Patterson, R. Sougrat, O. Wolf Lindwasser, S. Olenych, J. S. Bonifacino, M. W. Davidson, J. Lippincott-Schwartz, and H. F. Hess, Science **313**, 1642 (2006).

[2] M. J. Rust, M. Bates, and X. Zhuang, Nat. Methods **3**, 793 (2006).

[3] S. W. Hell and J. Wichmann, Opt. Lett. **19**, 780 (1994).

[4] S. W. Hell, Science **316**, 1153 (2007).

[5] A. Volkmer, J. Phys. D **38**, R59 (2005).

[6] J. X. Cheng, Appl. Spectrosc. **61**, 197A (2007).

[7] K. A. Stankov and V. P. Tzolov, Appl. Phys. B **52**, 96 (1991).

[8] G. Marowsky and G. Lüpke, Appl. Phys. B **51**, 49 (1990).

[9] E. S. Lee and J. W. Hahn, Appl. Opt. **33**, 8302 (1994).

[10] E. O. Potma, C. L. Evans, and X. S. Xie, Opt. Lett. **31**, 241 (2006).

[11] M. Jurna, J. P. Korterik, C. Otto, and H. L. Offerhaus, Opt. Express **15**, 15207 (2007).

[12] E. S. Lee, J. Y. Lee, and Y. S. Yoo, J. Biomed. Opt. **12**, 024010 (2007).

[13] C. L. Evans, E. O. Potma, and X. S. Xie, Opt. Lett. **29**, 2923 (2004).

[14] D. L. Marks and S. A. Boppart, Phys. Rev. Lett. **92**, 123905 (2004).

[15] S. H. Lim, A. G. Caster, and S. R. Leone, Phys. Rev. A **72**, 041803(R) (2005).

[16] T. W. Kee, H. Zhao, and M. T. Cicerone, Opt. Express **14**, 3631 (2006).

[17] C. Vinegoni, J. S. Bredfeldt, D. L. Marks, and S. A. Boppart, Opt. Express **12**, 331 (2006).

[18] V. V. Krishnamachari and E. O. Potma, J. Raman Spectrosc. **39**, 593 (2007).

[19] V. V. Krishnamachari, E. R. Andresen, S. R. Keiding, and E. O. Potma, Opt. Express **14**, 5210 (2006).

[20] S. A. J. Druet and J. P. E. Taran, Prog. Quantum Electron. **7**, 1 (1981).

[21] H. Wang, Y. Fu, and J. X. Cheng, J. Opt. Soc. Am. B **24**, 544 (2007).

[22] V. V. Krishnamachari and E. O. Potma, J. Opt. Soc. Am. A **24**, 1138 (2007).

[23] V. V. Krishnamachari and E. O. Potma, Chem. Phys. **341**, 81 (2007).

[24] E. O. Potma, W. P. de Boeij, and D. A. Wiersma, J. Opt. Soc. Am. B **17**, 1678 (2000).